Growth of multiwall carbon nanotubes in an inductively coupled plasma reactor

Lance Delzeit, Ian McAninch,[a] Brett A. Cruden,[b] David Hash, Bin Chen,[b] Jie Han, and M. Meyyappan[c]
NASA Ames Research Center, Moffett Field, California 94035

(Received 5 December 2001; accepted for publication 5 February 2002)

A high density plasma from a methane–hydrogen mixture is generated in an inductively coupled plasma reactor, and multiwalled carbon nanotubes (MWNTs) are grown on silicon substrates with multilayered Al/Fe catalysts. The nanotubes are vertically aligned, and the alignment is better than the orientation commonly seen in thermally grown samples. A detailed parametric study varying inductive power, pressure, temperature, gas composition, catalyst thickness, and power to the substrate is undertaken. Transmission electron microscopy and Raman spectroscopy are used to characterize the nanotubes. Emission spectroscopy and a global model are used to characterize the plasma. The power in the lower electrode holding the substrate influences the morphology and results in a transition from MWNTs to nanofibers as the power is increased. © *2002 American Institute of Physics.* [DOI: 10.1063/1.1465101]

I. INTRODUCTION

Chemical vapor deposition (CVD) has become a common technique recently to grow multiwalled[1] and singled-walled[2] carbon nanotubes. It provides a simple approach to grow nanotubes on patterned substrates and proceeds at temperatures below 1000 °C, substantially lower than in laser ablation and carbon arc processes. Hydrocarbon or CO feedstock is passed over substrates catalyzed with transition metals to facilitate the growth of nanotubes. More recently low temperature plasmas have been used in growing multiwalled carbon nanotubes (MWNTs).[3–14] The conventional wisdom for plasma processing in microelectronics is that it allows preparation of thin films at substrate temperatures significantly lower than that possible with thermal CVD. Such an advantage is highly desirable in many applications that stand to lose certain characteristics of the processed wafer at elevated temperatures (for example, charring of the photoresist). This wisdom does not entirely transfer to the use of plasmas in nanotube growth since the catalyst activation requires temperatures of at least 550 °C. For example, carbon nanotubes cannot be grown at a substrate temperature of 100 °C in a plasma environment. Then the purpose of the plasma and advantage, if any, over thermal CVD are not clear and none of the Refs. 3–13 address this issue. It may very well be that the plasma is another alternative to dissociate the feedstock gases, perhaps more efficiently. For example, a microwave plasma at 1 kW power level dissociates CH_4 with a high degree of conversion. However, it is not clear now if such a thorough conversion is required based on the fact that thermal CVD of nanotubes from methane is reported[2,15] at temperatures of 750–900 °C. The typical dissociation temperature for methane is about 1200 °C, and the extent of dissociation at 750 °C in a thermal CVD reactor is expected to be less than in a microwave reactor at 1 kW. At the core of this debate is the lack of identity of the carbon-bearing species near and on the catalyst particles as well as surface chemical mechanisms. Kanzow and Ding[16] and Sinnott *et al.*[17] have proposed models for nanotube growth, though issues of surface catalyzed reactions are not addressed.

Recently Zhou and coworkers[14] used a microwave methane/ hydrogen plasma and clearly showed that the plasma enabled a vertically oriented growth of MWNTs. In an elegant experiment, the growth run was first started with the plasma on and after a certain period, the plasma was turned-off and the growth was continued with the same substrate heating. While the nanotubes in the early period under plasma conditions exhibited a high degree of alignment, the continued growth under thermal conditions showed randomly oriented tubes. Indeed, when the electric field was deliberately induced at an angle, the nanotubes followed the field direction showing a tilted behavior. This is not surprising in view of the recent demonstration[18] that even in thermal CVD, introduction of an electric field with the aid of two electrodes clamped to the quartz tube (without striking a glow discharge) helped to align the nanotubes. The encouraging results in Ref. 14 suggest that the low temperature plasmas, particularly those with independent control of the substrate bias, can be useful in the growth of nanotubes in vertical alignment. In this work we have constructed an inductively coupled plasma (ICP) reactor with an independent rf power supply to the electrode holding the substrate. All previous works have used microwave,[4,6–10,14] hot filament,[3,5] or dc discharges.[13] ICP reactors are simple to construct and offer a high ionization efficiency compared to dc or rf capacitive discharges. In this work the effects of various process parameters such as pressure, methane–hydrogen com-

[a]Summer undergraduate intern from RPI.
[b]ELORET Corporation.
[c]Electronic mail: meyya@orbit.arc.nasa.gov

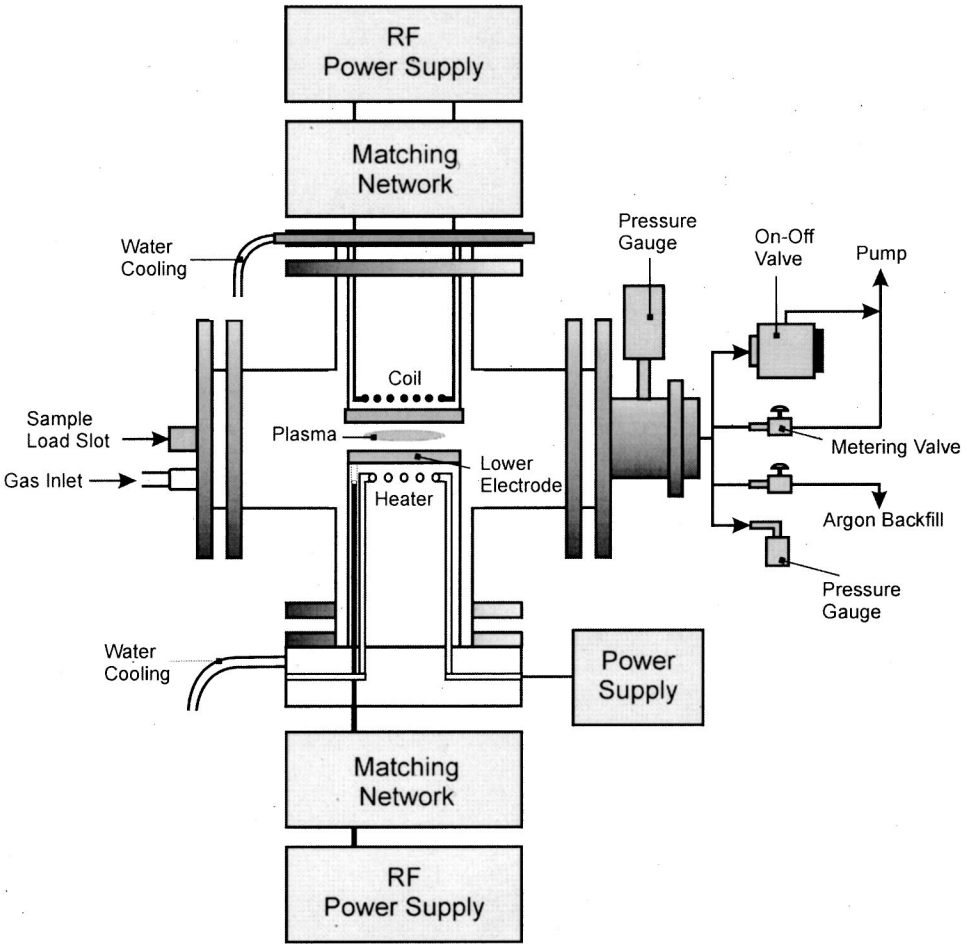

FIG. 1. Schematic of the plasma reactor.

position, argon dilution, catalyst thickness, temperature, inductive power, and substrate power on MWNT growth are addressed. The nanotubes are characterized using transmission electron microscopy (TEM) and Raman scattering. Limited diagnostics of the plasma using emission spectroscopy and a simple zero-dimensional model with comprehensive plasma chemistry are used to gain some understanding of the plasma characteristics.

II. EXPERIMENTAL WORK

Figure 1 shows a schematic of our ICP reactor consisting of a pair of electrodes mounted within a 25×25 cm Pyrex cross with 7.5 cm inner diameter. The two electrodes are 6.875 cm in diameter and 1.25 cm apart. The upper electrode consists of a six-turn copper coil that is inductively coupled to the plasma through a Pyrex coupling window. The Pyrex window is held on by a metallic ring that serves as a ground surface to the capacitively coupled lower electrode. The powered portion of the lower electrode is 6.25 cm in diameter. A ground shield with a 0.0625 cm spacing accounts for the remainder of the lower electrode assembly. The lower electrode is heated by a resistive coil heater and its temperature is monitored using a thermocouple and controlled by a temperature controller (Fuji Electric, FXZ-9). Both the lower electrode and inductive coil are powered by separate 13.56 MHz rf generators (Advanced Energy, RFX-600) with their associated matching networks (Advanced Energy, ATX-600). Gases are fed and controlled by MKS 1179A mass flow controllers. Pressure is measured with one of two transducers shown in the schematic (MKS 722A and 220BA) and controlled with a manual valve. The plasma commonly ignites in the arms of the cross, and thus comes in close contact with the pressure gauges. The pressure measured while the plasma is on is therefore unreliable, and all pressures reported in this work are those prior to plasma ignition.

Thin layers of Al followed by Fe were sputtered onto silicon substrates (*N*-doped, ⟨100⟩) by ion beam sputtering (VCR Group ion beam sputterer model IBS/TM2005). The reactor was continuously flushed with argon (99.999%) during loading and unloading of samples. Once the silicon substrate was in place, the reactor was pumped down to about 10^{-5} Torr and the substrate stage was heated up to the desirable temperature, allowing 10 minutes for temperature equlibration. Then the methane–hydrogen gas mixture (both gases 99.999% pure) was admitted and the reactor pressure was set to the desired value. The capacitive power to the lower electrode and the inductive power to the coil were turned on, and a plasma was ignited. A growth time of 10 min was used in this study and at the end, the reactor was allowed to cool (<300 °C) under vacuum before exposure to air.

While the growth was in progress, optical emission spectra were collected using a 50 cm monochromator (TVC Instruments, 82-050) installed with a photodiode array (PDA)

detector (Alton Instruments, LS2000). The acceptance cone of the spectrometer is large enough to include the entirety of the plasma between the electrodes. Peaks from several species are identified: the CH $A^2\Delta - X^2\Pi$ (0,0) band near 430 nm, the atomic H Balmer series (α peak at 680 nm and β peak at 486 nm), and a multitude of molecular H_2 peaks, with the strongest being at 464 nm. Other species expected to be present, such as CH_3 and atomic C, cannot be observed as the Pyrex tube does not transmit their emission in the ultraviolet region. The intensities reported in this work are the peak intensities of these bands. The nanotubes were characterized using scanning electron microscopy (SEM), TEM, and Raman spectroscopy. Raman analysis was conducted using a System 2000 micro-Raman spectrometer (Renishaw) in the backscattering configuration. A 2 to 3 MW laser power was used on the sample with a 1 μm focus spot at 50% power level to avoid photodecomposition of the sample. The total accumulation time was 30 s. A 514 nm argon ion laser and a 633 nm He–Ne laser were used for excitations. An 1800 lines/mm grating was used to achieve optimum resolution and throughput. The achieved resolution is better than 4 cm^{-1} in the 100–4000 cm^{-1} spectral window. Spectra were taken in at least three different spots to ensure the reproducibility of peak intensities. The spectrometer was calibrated with atomic emission from a neon lamp and checked with silicon lines before collecting the spectra.

III. MODEL

The analysis consists of a simple volume averaged or 0-dimensional (0-D) model of the plasma. The purpose of this model is to identify the components of the plasma and understand how they change as process parameters are varied. The knowledge derived from this exercise may be useful in generating some inferences regarding the observations from experiments. No attempt is made to model the nanotube growth itself since very little is known about the actual growth mechanism, surface reactions, etc., and the absence of both qualitative and quantitative information does not allow addressing this aspect. In contrast, electron impact dissociation of methane and hydrogen and neutral reactions are fairly well known in the literature, mainly from diamond deposition and combustion studies.

The 0-D model is a collection of mass balance equations for electrons, various ions, and neutral species along with gas energy and electron energy balance equations.[19] A computer code SAMPR described in Refs. 20 and 21 is used here to analyze the methane–hydrogen inductive discharge used in our experiments. The input to the code consists of reactor volume and surface area, flow rate and composition of the feed gases, pressure, power, reactions in the plasma with their rate data, and sticking coefficients for active species recombining on reactor surfaces. A total of 48 species (21 neutrals, 26 ions, and electrons) is included in the analysis. The homogeneous reaction set considered in this work is fairly comprehensive consisting of 563 reactions. The reaction set includes electron impact reactions (ionization, excitation, dissociation, dissociative ionization etc), ion–ion and electron–ion recombinations, ion–neutral charge exchange, and neutral reactions (abstraction, recombination, etc.). In typical microelectronics plasma processing operations at sub-100 mTorr and 500 K conditions, neutral reactions and a variety of recombination reactions would be negligible. Here at conditions of 1–20 Torr and 1000–1200 K, such reactions cannot be ignored.

IV. RESULTS AND DISCUSSION

The catalyst formulation used in this study, except when noted, involves 10 nm Al followed by 10 nm Fe, both sputtered from 99.9+% pure metals. The Al underlayer here, as shown in our previous works,[2,22] appears to provide more nucleation sites and has been demonstrated to be useful in growing both single walled carbon nanotubes (SWNTs) and MWNTs by thermal CVD. In Ref. 22 we have shown that the as-sputtered thin layer of Fe consists of particles less than 10 nm as imaged by an atomic force microscope with a 1 nm diameter SWNT probe. Others[5,8–14] who have used pure Fe or Ni as catalysts, prepared by physical processes such as magnetron sputtering, electron-beam evaporation, etc., had to resort to some form of pretreatment (for example, exposure to H_2 plasma and ion bombardment or etching using NH_3) to prepare the growth surface creating particles. When an underlayer is used, no such pretreatment is needed. Nolan *et al.*[23] suggest, in their study on the thermodynamics and kinetics of carbon deposition, that alloying a catalyst with a noncatalytic metal increases the number of reactive sites through surface clusters.

Our initial investigations focused on the temperature dependence of the nanotube growth. For MWNT growth using methane, 700–800 °C has been found to be good in thermal CVD.[22] Investigation within this range here shows that the growth rate at 800 °C is higher than at 700 °C and as a result, the growth temperature is fixed at 800 °C in all subsequent runs. The base conditions for this work evolved from efforts to grow vertically oriented specimens of reasonable density and electrical conductivity for use as electrodes in our sensor development work. These conditions are: 3 Torr, 20% CH_4 and 80% H_2 at a total flow of 100 sccm, 800 °C, 100 W inductive power, 70 W at the lower electrode, and 10 min of growth time. The parametric study involves perturbation of each of the above variables within a meaningful range while keeping other parameters fixed.

Figure 2 shows the growth characteristics as a function of substrate power which has the most dramatic effect of all the process variables. The range of power to the lower electrode holding the substrate is varied from 0 to 120 W. Power levels above 140 W are not investigated due to high reflected power. MWNTs which are only marginally aligned are seen at 0–20 W power levels. At 50 W and above, we see what we call multiwalled nanofibers which are well aligned. There is a transition at 30 and 40 W when nanotubes and nanofibers are mixed. The density of the nanofibers decreases as power is increased beyond 70 W. TEM images (Fig. 3) reveal that the diameter of MWNTs are 6–20 nm and the nanofibers are in the range of 20–30 nm. This distinction is made based on the definition given by Nolan *et al.*[23] A nanofiber or filament consists of a stacked cone-segment

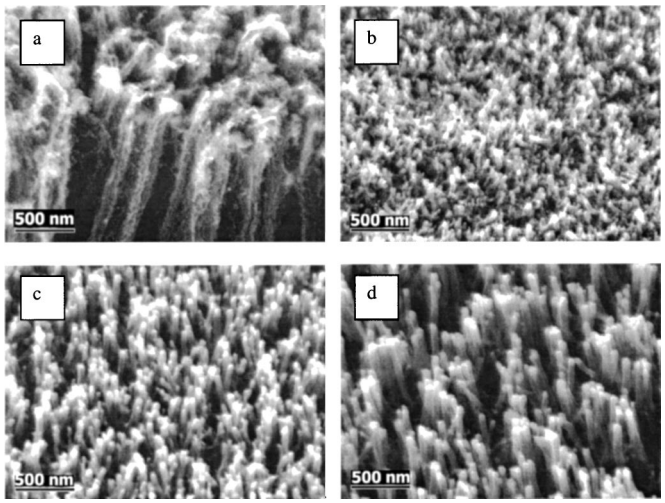

FIG. 2. Effect of rf power on the bottom electrode holding the substrate. Reactor conditions: 3 Torr, 100 W inductive power, 800 °C, 20:80 methane/H_2 mixture, and 100 sccm flow rate. 10 nm of Fe is used as a catalyst with an underlayer of 10 nm Al. (a) 20 W, (b) 40 W, (c) 50 W, and (d) 70 W.

shaped graphite basal plane sheets and grows with the catalyst particle at the tip. Nolan *et al.* suggest that hydrogen satisfies the valences at cone edges in such fibers. The orientation angle θ between the graphite basal plane and the tube axis is nonzero. A nanotube in contrast has its graphite basal plane parallel to the tube axis ($\theta = 0$) and the catalyst particle at the base. A nanotube has no graphite edges and therefore no need for valence-satisfying species such as hydrogen. Nolan *et al.* provide evidence that the material produced by CO disproportionation (without any H_2) is only multiwalled nanotubes and with the addition of H_2, fibers are produced. Indeed, as the percentage is increased, θ is seen to increase

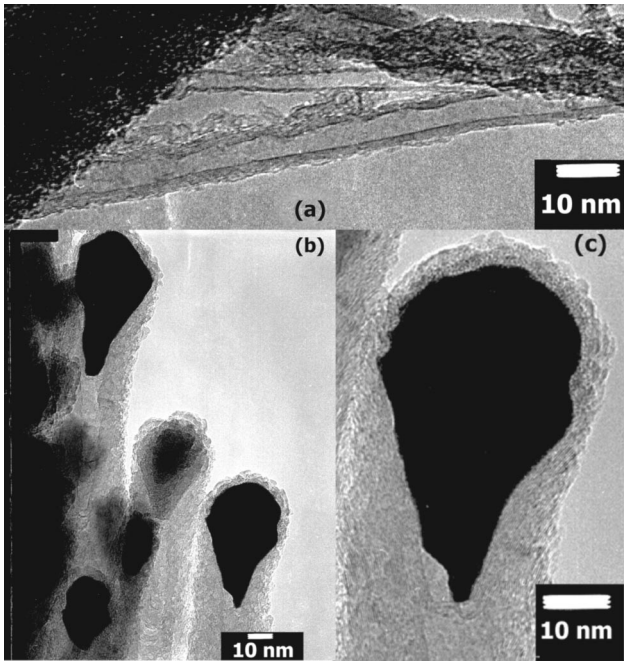

FIG. 3. TEM images. (a) HRTEM image of multiwalled nanotubes, (b) nanofibers, and (c) HRTEM image of a MWNF showing a pear-shaped particle at the tip.

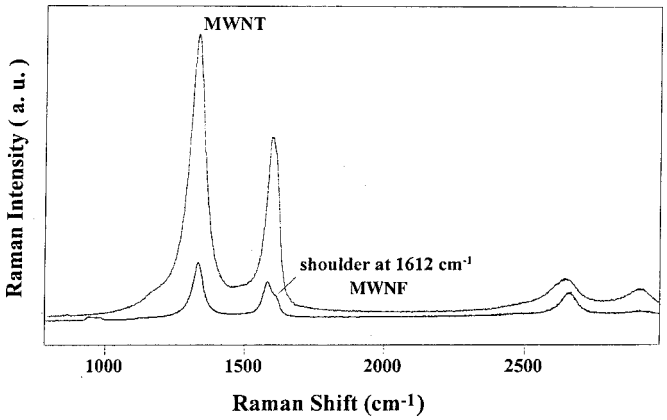

FIG. 4. Raman spectra at 633 nm excitation.

up to 30°.[23] It is important to note that these, as well as our, materials are not solid cylinders but are mostly hollow with small θ values. For this reason, it may be appropriate to call them multiwalled nanofibers (MWNFs) instead of graphitic carbon fibers (GCF) or vapor grown carbon fibers (VGCF) both of which denote solid cylinders in the literature.

The MWNTs [Fig. 2(a)] do not have particles at the top but appear to follow a base growth mechanism. They are generally thinner than the MWNFs. We even see a double-walled nanotube in the HRTEM image in Fig. 3. The TEM image of the MWNFs shows the stacked cone arrangement and the catalyst particle at the tip. The particle is shaped like a pear or tear drop and is about 25 nm at its widest point. Examination of the edges reveals that these MWNFs are free of amorphous carbon. Merkulov *et al.*[11] and Chen *et al.*[3] also showed similar TEM images with stacked cone interior and pear-shaped catalyst particles at the tip, and both appropriately called their material nanofibers to distinguish them from MWNTs. Our present work, however, is the first to show a transition from MWNT to MWNF by changing a process variable. Additional evidence of this transition is also provided by Raman scattering (Fig. 4). Both materials have a similar tangential *G* band centered at 1590 cm^{-1} (Ref. 24) and a *D* band centered at 1350 cm^{-1}. A prominent difference is noticed in MWNF samples in the form of a shoulder peak at 1616 cm^{-1} that is possibly related to the E2 mode. Because of the more curved folding of the graphite sheet to form the fiber compared to MWNT, this inactive Raman mode becomes optically allowed due to the broken symmetry. Its origin needs further theoretical study. Secondary bands for both samples are similar except the redshift of secondary *G* bands in the MWNTs which are narrower than in the MWNFs. The results are similar from both 514 and 633 nm excitations.

Increasing the power to the lower electrode from 0 to 120 W increases the self-dc bias at the substrate from a small value to about −400 V. The dc bias at the substrate, which affects the local environment such as the sheath electric field, ion energy, etc., depends on the materials of the electrode, wafer, and the layers on the wafer, for a given power at the electrode and other fixed plasma parameters. Since we are interested in aligned nanotubes as electrodes for sensor de-

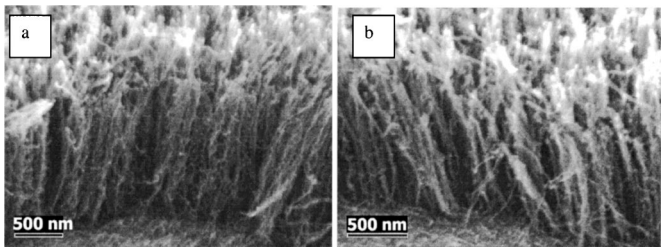

FIG. 5. SEM images of MWNTs when (a) 10 nm Ir and (b) 10 nm Mo is added to 10 nm Fe/10 nm Al as an additional underlayer. The substrate rf power is 70 W. All other conditions are the same as in Fig. 3. Without the Ir or Mo layer, MWNFs result [see Fig. 3(d)] under identical conditions.

velopment, additional or alternative underlayers may be of interest to enhance the conductivity. Figure 5 shows growth results for the base conditions (70 W at the lower electrode) when a 10 nm Ir or Mo is added to the standard 10 nm Al/10 nm Fe. These are clearly MWNTs while at the same conditions Al/Fe layers provided MWNFs. Indeed, when the power is increased to 100 W, well-aligned MWNFs [similar to Fig. 2(d)] are again obtained (not shown here). The addition of an Ir or Mo layer effectively pushes the transition from MWNTs to MWNFs to a higher power (~80 W). It is noteworthy that there is not a significant change in plasma emission with the above variations, suggesting the transition is not due to plasma chemistry but due to the multilayer formulation.

The emission results collected from all the growth runs, plotted in Fig. 6, provide an interesting correlation to the observed transition. The growth of nanotubes is accompanied by a low peak intensity of atomic hydrogen and as the hydrogen emission intensity increases, nanofibers are obtained. This observation is consistent with the analysis of Nolan *et al.*[23] The H peak intensity increases steadily with power to the lower electrode. This may be due to the increased dissociation of H_2 resulting from possible increases in electron density and temperature at a fixed inductive power and pressure. The 0-D model shows that the electron temperatures of pure inductive discharges at pressures of 3–20 Torr are rather low at about 1.75 eV and the electron density is $\sim 10^{11}$ cm^{-3}. The addition of capacitive power to the bottom electrode can increase these values, thus increasing electron impact dissociation of H_2. If a large amount of argon is added as a diluent, MWNTs are formed as shown in Fig. 7. The corresponding H intensities, in the regime favoring MWNTs, are lower as seen in Fig. 6(b) since excessive dilution with argon would reduce the H_2 as well as H fractions.

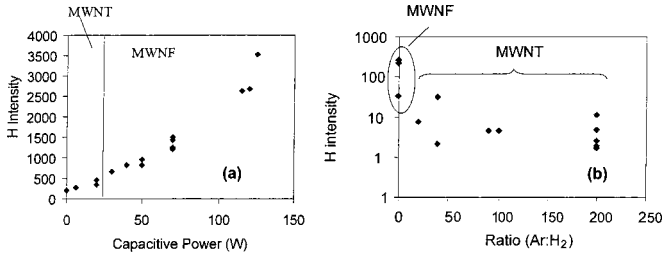

FIG. 6. Atomic hydrogen intensity from emission spectroscopy. (a) Variation with substrate power and (b) effect of argon dilution.

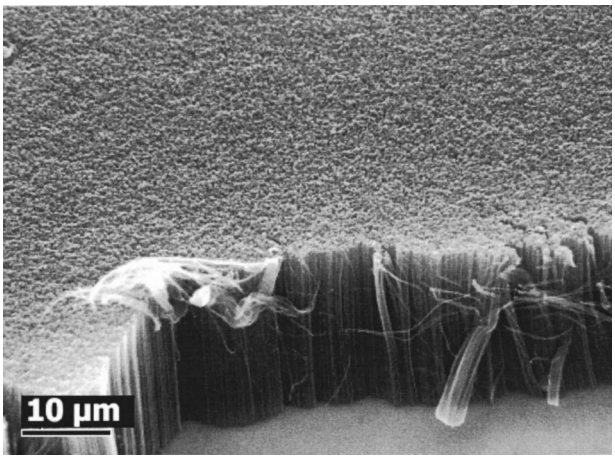

FIG. 7. SEM image of MWNTs grown with argon addition. Growth conditions: 20 Torr; 50/50/1000 sccm of $CH_4/H_2/Ar$; 100 W inductive power; 100 W rf power to the substrate; 800 °C; 10 min growth time; observed self-bias ~−5 V; and the catalyst formulation is 10 nm Fe/10 nm Al.

In the absence of argon addition, nanofiber growth is common when methane is varied from 1% to 20% in the CH_4-H_2 mixtures, keeping other parameters at their base values; this may be due to the 70 W capacitive power in the base conditions being favorable to growing MWNFs as discussed before. The diameter of the fibers does not seem to be affected by the methane fraction. 20% methane provides a good density of fibers. Emission measurements show an increase in CH intensity with methane fraction as expected. But the atomic hydrogen intensity does not vary much with the flow ratio. Electron temperature, estimated from the ratio of the β and α hydrogen emission lines, also seems to be invariant with flow ratio. These observations are consistent with the 0-D results. We note that most of the plasma grown material reported in the literature[5–10,12–14] appear to be MWNFs (though they were called MWNTs in these references) with diameters in the range of 20–100 nm and all with pear-shaped catalyst particles at the tip. Most of these works did not show any HRTEMs defining the morphology. Zhang *et al.*[7] observed in the Raman spectra of their samples the same shoulder peak as in Fig. 4 at 1620 cm^{-1} but did not recognize nanofibers. Interestingly, the common feedstock in all the studies is methane (or acetylene) diluted heavily (1% to 2% hydrocarbon) with H_2 (or NH_3 sometimes) which has its origin in diamond growth. These discharges produce copious amounts of atomic hydrogen (see Table I for representative neutral species densities) which results in MWNFs as discussed above. It is important to note that the nanofibers are well aligned and useful as electrodes and field emitters as reported in Refs. 5, 9, and 11.

Figure 8 shows the effect of pressure on growth characteristics. A large amount of amorphous carbon contamination is seen at pressures of 20 Torr and above. This is not a problem at low pressures but the density of the MWNFs is low at pressures below 1 Torr. MWNFs of uniform height and density are obtained at 3 Torr which seems to be the optimum when all other parameters are at their base values. A decrease in electron temperature accompanies an increase in pressure as revealed by the emission data and the model,

TABLE I. Densities (in cm^{-3}) of key neutral species from the 0D model. Conditions: 3 Torr, 800 °C, 100 W inductive power, and 100 sccm flow of 20:80 methane/hydrogen.

H_2	2.47×10^{16}	C_2	1.45×10^{10}	C_3H_2	8.11×10^{10}
H	4.60×10^{14}	C_2H	1.38×10^{10}	C_3H_3	4.46×10^{10}
CH_4	1.34×10^{15}	C_2H_2	2.10×10^{14}	C_3H_4	1.33×10^{11}
CH_3	2.70×10^{14}	C_2H_3	2.72×10^{11}	C_3H_5	2.03×10^{10}
CH_2	1.72×10^{10}	C_2H_4	6.72×10^{13}	C_3H_6	1.18×10^{12}
CH	1.38×10^{9}	C_2H_5	1.86×10^{12}	C_3H_7	4.21×10^{10}
C	3.01×10^{9}	C_2H_6	6.51×10^{13}	C_3H_8	8.51×10^{11}

which is a well-known behavior.[19] The densities of feedstock gases, CH_4 and H_2, increase with pressure. Nevertheless, the decreases in electron density and electron temperature lead to a decrease in most of the neutrals shown in Table I except C_2H_2, C_2H_4, and C_2H_6. Though radical densities decrease from 1 to 20 Torr, reasonable growth is still possible due to the availability of CH_4, C_2H_2, C_2H_4, and C_2H_6 for decomposition at the catalyst particle surface. The amorphous carbon problem at high pressures may be related to the excessive supply of these carbon sources. The effect of inductive power is also studied between 0 and 200 W with all other parameters at their base values. Note that when the inductive power is zero, the plasma is entirely powered by the 70 W capacitive power at the bottom electrode. As seen in Fig. 9, there is a small effect on the density of growth as the inductive power is turned on, and a further increase in power at these conditions seems to have minimal impact.

It is of interest to know the effect of catalyst layer thickness on growth characteristics. Our previous studies on thermal CVD with the same catalyst formulation demonstrated[2,22] that the density of growth can be controlled by varying the thickness of the underlayer and catalyst layers, but the effect on diameter selection is minimal. Here, the Fe layer thickness is varied between 1 and 40 nm, keeping the Al underlayer at 10 nm. A minimum of 5 nm of Fe seems to be required to initiate growth. Reasonable densities of MWNFs at base conditions are obtained with 10 nm Fe as seen throughout this work. Increasing the Fe layer thickness beyond 10 nm yields nanofibers with bigger diameters; for example, a 40 nm Fe layer results in MWNFs with a 75 nm diameter. This would allow one to tune the diameter based on applications needs. The present dependence of diameter on catalyst film thickness is consistent with the results of Wei *et al.*[25] who compared thermal CVD and dc plasma CVD with the same catalyst in a careful study. While there is no apparent dependence of diameter on catalyst thickness in thermally grown samples, their plasma grown samples varied from 50 nm diameter for a 10 nm catalyst layer to 300 nm for a 40 nm catalyst.

V. CONCLUDING REMARKS

We have used an inductively coupled plasma reactor to grow carbon nanotubes. Our reactor is a small, homemade version of the large, commercial ICP reactors widely used in the semiconductor industry. The ICP source is efficient in terms of power utilization and ionization, as in the microwave sources popularized by the diamond community. Both sources have an additional capacitive rf or dc power source coupled to the bottom electrode holding the substrate to provide an independent control of the ion flux and energy. Varying this power, we have shown that a transition occurs from multiwalled nanotubes to multiwall nanofibers. These nanofibers are not solid cylinders but are mostly hollow with the graphite basal plane at a small angle to the tube axis.

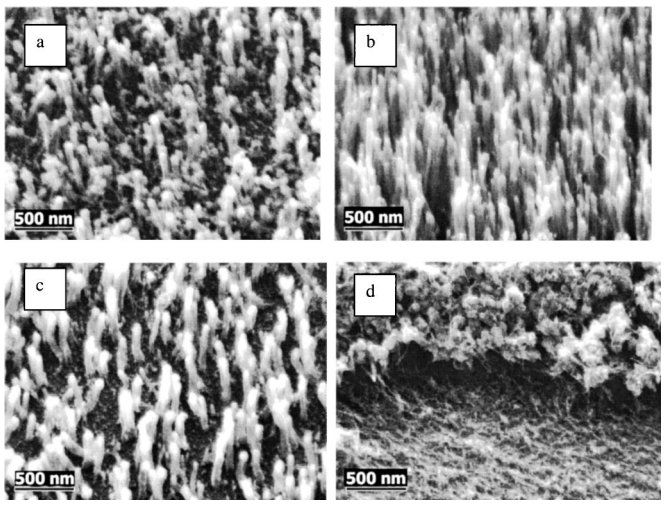

FIG. 8. Effect of pressure on MWNF growth. Substrate power is set at 70 W with all other conditions as in Fig. 3. (a) 0.5 Torr, (b) 3 Torr, (c) 10 Torr, and (d) 20 Torr.

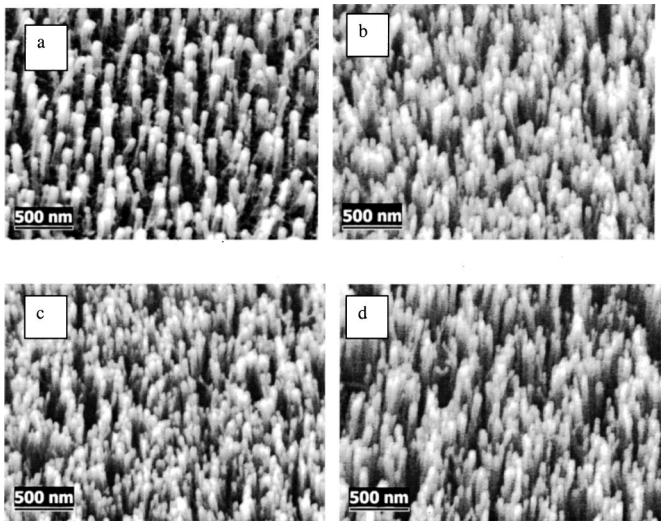

FIG. 9. Effect of inductive power on growth characteristics. Substrate rf power is fixed at 70 W with all other conditions as in Fig. 3. (a) 0 W, (b) 50 W, (c) 100 W, and (d) 200 W.

Both HRTEM and Raman spectroscopy provide evidence distinguishing MWNTs from MWNFs. The nanotubes grow with catalyst particles at the bottom whereas the nanofibers have pear-shaped catalyst particles at the tip. The nanotubes range from double-walled to 20 nm in diameter. The nanofibers in this work are mostly 20–30 nm in diameter and by increasing the catalyst layer thickness, larger 75 nm nanofibers are obtained. Finally, the nanofibers are much more vertically aligned than the nanotubes.

The regimes producing the MWNFs coincide with the availability of large amounts of atomic hydrogen which is common in hydrocarbon discharges with H_2. Replacing H_2 with argon favors production of MWNTs. The vertically aligned MWNFs with controllable densities and diameters are suitable for development of electrodes and field emitters.

A simple 0-D model suggests that the discharge produces large amounts of atomic hydrogen along with a variety of C_xH_y radicals. Stable species such as CH_4, C_2H_2, C_2H_4, etc., account for about 5% in a 20:80 CH_4/H_2 discharge at 3 Torr. The radicals and higher order stable species such as C_2H_2 and C_2H_4 decompose on catalyst particle surfaces at lower temperatures than methane to produce the solid carbon needed for nanotube or nanofiber growth. The primary chemical role of the plasma seems to be the production of atomic hydrogen through electron impact dissociation of H_2. The production of methyl radical is overwhelmingly from the hydrogen abstraction reaction $(CH_4+H\rightarrow CH_3+H_2)$ compared to electron impact dissociation of methane. The 0-D model is useful to identify the nature of neutrals and ionic species in the reactor and generate global scaling laws of plasma properties with process variables. More detailed two-dimensional models are needed to probe the local environment near the growth surface, and the effect of the ions and the self-bias generated at the bottom electrode, which is currently being pursued. Such detailed models are amenable for comparison with the thermal CVD process. *In situ* diagnostics of the plasma and wafer surface are important for model validation as well as to gain understanding of the growth process. Low temperature plasma processing is complex and such two-pronged fundamental investigations involving modeling and diagnostics have been long recognized by the silicon semiconductor processing community.

ACKNOWLEDGMENTS

The authors acknowledge Jeff Ifland for his excellent work on construction of the reactor and instrumentation. Surendra Sharma and M.V.V.S. Rao are acknowledged for their valuable suggestions on reactor design and diagnostics. The work by ELORET authors is supported by NASA Contract No. NAS2-99092.

[1] M. Su, B. Zheng, and J. Liu, Chem. Phys. Lett. **322**, 321 (2000), and references therein.
[2] L. Delzeit, B. Chen, A. M. Cassell, C. Nguyen, and M. Meyyappan, Chem. Phys. Lett. **348**, 368 (2001), and references therein.
[3] Y. Chen, Z. L. Wang, J. S. Yin, D. J. Johnson, and R. H. Prince, Chem. Phys. Lett. **272**, 178 (1997).
[4] L. C. Qin, D. Zhou, A. R. Krauss, and D. M. Gruen, Appl. Phys. Lett. **72**, 3437 (1998).
[5] Z. F. Ren, Z. P. Huang, J. W. Xu, J. H. Wang, P. Bush, M. P. Siegel, and P. N. Provencio, Science **282**, 1105 (1998).
[6] S. H. Tsai, C. W. Chao, C. L Lee, and H. C Shin, Appl. Phys. Lett. **74**, 3462 (1999).
[7] Q. Zhang, S. F. Yoon, J. Ahn, B. Gan, Rusli, and M. B. Yu, J. Phys. Chem. Solids **61**, 1179 (2000).
[8] Y. C. Choi, Y. H. Lee, B. S. Lee, G. Park, W. B. Choi, N. S. Lee, and J. M. Kim, J. Vac. Sci. Technol. A **18**, 1864 (2000).
[9] Y. C. Choi, Y. M. Shin, S. C. Lim, D. J. Bae, Y. H. Lee, B. S. Lee, and D. Chung, J. Appl. Phys. **88**, 4898 (2000).
[10] M. Okai, T. Muneyoshi, T. Yaguchi, and S. Sasaki, Appl. Phys. Lett. **77**, 3465 (2000).
[11] V. I. Merkulov, D. H. Lowndes, Y. Y. Wei, G. Eres, and E. Voelkl, Appl. Phys. Lett. **76**, 3555 (2000).
[12] G. W. Ho, A. T. S. Wee, J. Lin, and W. C. Tjiu, Thin Solid Films **388**, 73 (2001).
[13] K. B. K. Teo, M. Chhowalla, G. A. J. Amaratunga, W. I. Milne, D. G. Hasko, G. Pirio, P. Legagneux, F. Wyczisk, and D. Pribat, Appl. Phys. Lett. **79**, 1534 (2001).
[14] C. Bower, W. Zhu, S. Jin, and O. Zhou, Appl. Phys. Lett. **77**, 830 (2000).
[15] J. Kong, H. T. Soh, A. M. Cassell, C. F. Quate, and H. Dai, Nature (London) **395**, 878 (1998).
[16] H. Kanzow and A. Ding, Phys. Rev. B **60**, 11180 (1999).
[17] S. B. Sinnott, R. Andrews, D. Qian, A. M. Rao, Z. Mao, E. C. Dickey, and F. Derbyshire, Chem. Phys. Lett. **315**, 25 (1999).
[18] Y. Avigal and R. Kalish, Appl. Phys. Lett. **78**, 2291 (2001).
[19] M. A. Lieberman and A. J. Lichtenberg, *Principles of Plasma Discharges and Materials Processing* (Wiley, New York, 1994).
[20] M. Meyyappan and T. R. Govindan, SAMPR: A Computer Code for Simple Analysis of Materials Processing Reactors, NASA Research Publication 1402, NASA (1997).
[21] S. Panda, D. J. Economou, and M. Meyyappan, J. Appl. Phys. **87**, 8323 (2000).
[22] L. Delzeit, C. V. Nguyen, B. Chen, R. Stevens, A. Cassell, J. Han, and M. Meyyappan, *J. Phys. Chem. B* (to be published).
[23] D. Nolan, D. C. Lynch, and A. H. Cutler, J. Phys. Chem. B **102**, 4165 (1998).
[24] C. Thomsen, Phys. Rev. B **61**, 4542 (2000).
[25] Y. Y. Wei, G. Eres, V. I. Merkulov, and D. H. Lowndes, Appl. Phys. Lett. **78**, 1394 (2001).